THE ASTROPHYSICAL JOURNAL, 565:1312–1322, 2002 February 1
© 2002. The American Astronomical Society. All rights reserved. Printed in U.S.A.

THE EFFECT OF COHERENT SCATTERING ON RADIATIVE LOSSES IN THE SOLAR Ca II K LINE

H. UITENBROEK
National Solar Observatory/Sacramento Peak,[1] P.O. Box 62, Sunspot, NM 88349; huitenbroek@nso.edu
Received 2001 September 7; accepted 2001 October 1

ABSTRACT

We investigate the influence of partial frequency redistribution (PRD) on radiative cooling due to the Ca II K line in a hydrostatic model of the quiet Sun, and in a series of 20 snapshots from a chromospheric radiation-hydrodynamics simulation. The net radiative rates in the K line were calculated through these models with three different frequency-redistribution formalisms: complete redistribution (CRD), angle-averaged PRD, and angle-dependent PRD. It is found that the approximation of CRD generally leads to an overestimate of the net radiative rates because of its neglect of coherent scattering. Compared to the more realistic full angle-dependent solution, angle-averaged PRD provides accurate emergent profiles and cooling rates in the hydrostatic model and also provides accurate instantaneous profiles in the dynamical snapshots, even when considerable macroscopic velocities are present. Instantaneous angle-averaged cooling rates in the dynamical snapshots may be different at times, but on average, cooling is very similar to the angle-dependent case. In the temperature minimum, the Ca II K line provides, on average, more cooling in the dynamic chromosphere at the same column mass than in the hydrostatic model. It provides less cooling in the chromosphere. Finally, we formulate an approximation for angle-averaged redistribution in a moving atmosphere, employing the unshifted redistribution function. This approximation is easy to implement in existing numerical codes and should provide an efficient method for PRD transfer solutions in dynamic models without loss of accuracy in emergent profiles and radiative cooling rates.

Subject headings: line: formation — methods: numerical — radiative transfer — shock waves — Sun: atmosphere — Sun: chromosphere

1. INTRODUCTION

The resonance lines of singly ionized calcium, the Fraunhofer H and K lines, are the two strongest lines in the optical part of the solar spectrum. With their broad wings and collisionally dominated excitation, they provide temperature diagnostics over a wide range of heights in the solar atmosphere. The lines have been employed extensively in determining the temperature structure of semiempirical models (Vernazza, Avrett, & Loeser 1981; Maltby et al. 1986; Fontenla, Avrett, & Loeser 1991, 1993) and in assessing the validity of chromospheric radiation-hydrodynamic models (Rammacher & Ulmschneider 1992; Carlsson & Stein 1992, 1995). In both types of modeling, the H and K lines also provide a significant contribution to the radiative heating and/or cooling of the upper layers of the atmosphere, but the energy gains and losses in the models are incorporated very differently. In the semiempirical models, the net radiative rates are calculated after the fact to evaluate the mechanical heating or cooling required to explain the determined thermal structure, while in the dynamical simulations, the atmospheric structure is a direct result of the calculated radiative and mechanical gains and losses. Clearly, a precise determination of the radiative losses in the Ca II resonance lines is a prerequisite for accurate conclusions on the structure of the chromospheric layers in both types of modeling.

It is well known that the H and K lines have to be treated with the partial frequency redistribution (PRD) formalism for diagnostic purposes (e.g., Shine, Milkey, & Mihalas 1975; Uitenbroek 1989a), and most likely the same holds true for energy-balance considerations (e.g., Huenerth & Ulmschneider 1995). Compared to complete frequency redistribution (CRD), which is sufficiently accurate for most weaker lines, PRD adds considerably to the complexity of radiative line transfer because the emission-profile coefficient depends on the radiation field directly, not only indirectly through the population numbers. This increases the nonlinearity of the transfer problem. The added complexity may even be greater in dynamic atmospheres, where the coupling between angles and frequencies introduced by macroscopic velocities could require the use of angle-dependent PRD instead of the computationally simpler angle-averaged variant. Often these added complications and the associated demand on computer resources have prevented the application of PRD in the numerical modeling of strong lines or have prompted the use of computationally cheaper, but less accurate, approximations. Carlsson & Stein (1992), for instance, use CRD in their treatment of strong lines to expedite their simulations, although they mimic the effects of coherent scattering in the Lyman lines by truncating the profiles at six Doppler widths. It is difficult to estimate, however, to what extent these approximations come at the expense of less accurate profiles, diminished diagnostic value, and less precise estimates of radiative rates, before actual calculations using full angle-dependent PRD are performed. This is the aim of the present paper.

Current computer workstations in combination with efficient numerical codes are now fast enough to investigate PRD line formation in dynamic atmospheres in a routine fashion, even with angle-dependent redistribution. The numerical method used in this paper is based on the angle-averaged code described by Uitenbroek (2001), adapted for angle-dependent PRD as described below. It employs preconditioning of the statistical equilibrium equations rather than linearization, which unfortunately makes it more diffi-

[1] Operated by the Association of Universities for Research in Astronomy, Inc. (AURA), for the National Science Foundation.

cult to implement in dynamical schemes that explicitly use such a numerical scheme. Nevertheless, this code allows us to estimate the difference between radiative losses in CRD and PRD through a series of snapshots from a radiation-hydrodynamics simulation (Carlsson & Stein 1999) by comparing the properties of transfer solutions with either formalism after the fact. Because the back-coupling of the transfer solution onto the dynamics of the simulation is ignored here, the PRD solution is most likely inconsistent with the energy balance in the simulation, at least when the derived net radiative rates differ appreciably from the CRD values. However, if the latter is the case, then the conclusion should nonetheless be that transfer with PRD is needed to accurately estimate radiative line cooling.

The validity of the angle-averaged PRD approximation in a one-dimensional plane-parallel atmosphere was investigated by Milkey, Shine, & Mihalas (1975), who found that even close to the limb, the difference with a full angle-dependent solution was less than 1% for the H and K lines. To simplify the computationally intensive task of angle-dependent PRD, these authors chose to adopt a two-level atomic calcium model with a depth-independent Doppler broadening and Voigt parameter, so that the same set of redistribution weights could be used at all locations in the atmosphere. They suggested that even though angle-averaged PRD seems appropriate in a static one-dimensional model, it may not be as accurate in a multidimensional inhomogeneous atmosphere or in an atmosphere with macroscopic velocity fields. In such cases, the radiation field is much more likely to be anisotropic and may require the more sophisticated angle-dependent treatment. Estimates for the effect of PRD on line cooling by the Mg II k line in atmospheres with shocks have been given by Huenerth & Ulmschneider (1995), who used angle-dependent redistribution with only one angle point, and a two-level magnesium atom. These authors conclude that PRD cooling rates are significantly smaller than CRD rates and are much more concentrated in narrow regions directly behind the shocks.

In this paper the validity of the angle-averaged approximation and its effect on the net radiative rates in the K line are investigated in a static atmosphere and through a set of dynamic simulation snapshots. In all cases, we account for the full depth dependence of the collisional and thermal line broadening and for the multilevel interactions in the calcium atom. Although the solution of the transfer equation in the comoving frame would require much less angle-quadrature points when macroscopic velocities are present (e.g., see Mihalas et al. 1976), we treat angle-dependent scattering in the observer's frame, because it is better suited to the nonmonotonic velocities that are present in the dynamical chromosphere. Bruls & Solanki (1997) modified the PRD code of Hubený & Lites (1995) for angle-dependent redistribution to investigate the effect of coherent scattering on the Stokes profiles of the H and K lines. Their results show only small sensitivity of the emerging intensity profiles to the number of angle-quadrature points, even when considerable macroscopic velocities are present in the atmosphere.

This paper is set up as follows. The equations for angle-dependent PRD and angle-averaged PRD in moving atmospheres are formulated in § 2. In § 3 the difference in radiative cooling due to the Ca II K line between CRD and angle-averaged and angle-dependent PRD is investigated in a hydrostatic model of the quiet Sun and in a series of snapshots from a hydrodynamic simulation. Conclusions are given in § 4.

2. ANGLE-DEPENDENT FREQUENCY REDISTRIBUTION

When the inner wings of a line form (i.e., have optical depth near unity) at a location in the atmosphere where radiative excitation in the line dominates over collisional excitation, effects of coherent scattering have to be taken into account. In this case, the emission-profile coefficient ψ of a line with upper level j and lower level i depends directly on the radiation field in the line and is given by (e.g., Uitenbroek 2001)

$$\psi_{ij}(\nu, \boldsymbol{n}) = \phi_{ij}(\nu, \boldsymbol{n})\left\{1 + \gamma \frac{n_i B_{ij}}{n_j P_j} \oint \frac{d\Omega'}{4\pi} \int d\nu' I(\nu', \boldsymbol{n}') \times \left[\frac{R^{\mathrm{II}}_{iji}(\nu, \boldsymbol{n}; \nu', \boldsymbol{n}')}{\phi_{ij}(\nu, \boldsymbol{n})} - \phi_{ij}(\nu', \boldsymbol{n}')\right]\right\} . \quad (1)$$

Here R^{II}_{iji} is the laboratory frame redistribution function corresponding to coherent scattering in the atom's frame, ϕ_{ij} is the absorption (and CRD emission) profile coefficient, γ is the coherency fraction, and P_j is the total depopulation rate of level j:

$$P_j = \sum_{k \neq j} (C_{jk} + R_{jk}) . \quad (2)$$

The terms C_{jk} and R_{jk} denote the collisional and radiative rate from level j to k, respectively.

Hummer (1962) provides an expression for the redistribution function $R^{\mathrm{II}}_{iji}(\nu, \boldsymbol{n}; \nu', \boldsymbol{n}')$ as a function of the reduced frequencies x, x' and the directions $\boldsymbol{n}$, $\boldsymbol{n}'$ of the outgoing and incoming photons, respectively:

$$(4\pi)^{-2} R^{\mathrm{II}}_{iji}(x, \boldsymbol{n}; x', \boldsymbol{n}') = \frac{g(\boldsymbol{n}, \boldsymbol{n}')}{4\pi^2 \sin \beta} \times \exp\left[-\left(\frac{x - x'}{2}\right) \csc^2 \frac{\beta}{2}\right] \times H\left(a \sec \frac{\beta}{2}, \frac{x + x'}{2} \sec \frac{\beta}{2}\right) . \quad (3)$$

Here β is the angle between the incoming and outgoing photon directions $\boldsymbol{n}'$ and $\boldsymbol{n}$, i.e., $\cos(\beta) = \boldsymbol{n} \cdot \boldsymbol{n}'$; $H(a, x)$ is the well-known Voigt function; a is the familiar ratio of line broadening over Doppler width; x and x' are frequencies from line center measured in Doppler widths; and $g(\boldsymbol{n}, \boldsymbol{n}')$ is the angular phase function for which we employ the dipole phase function

$$g(\boldsymbol{n}, \boldsymbol{n}') = \frac{3}{16\pi} (1 + \cos^2 \beta) . \quad (4)$$

Note that the redistribution function in equation (3) depends on direction only through the relative photon angle β. The normalization of the redistribution function given in equation (3) differs from the definition given by Hummer (1962, eq. [2.0.1]) by a factor of $(4\pi)^{-2}$, since we have chosen a different normalization of the redistribution function:

$$\oint\oint \frac{d\Omega'}{4\pi} \frac{d\Omega}{4\pi} \iint d\nu' \, d\nu \, R_{kji}(\nu', \boldsymbol{n}'; \nu, \boldsymbol{n}) \equiv 1 . \quad (5)$$

If we assume that the radiation at any particular part of the atmosphere is essentially isotropic, i.e., $I(\nu, \boldsymbol{n}) \approx J(\nu)$ for

all directions $\boldsymbol{n}$, where J is the angle-averaged mean intensity, then the integrals over frequency and angle in equation (1) can be carried out independently, and we speak of angle-averaged redistribution (cf., Mihalas 1978). It is by far the most computationally inexpensive way to incorporate coherent scattering effects, because convenient analytical expressions have been derived for the angle-averaged redistribution function R (e.g., Hubený 1982), which can be evaluated very efficiently (e.g., Gouttebroze 1986; Uitenbroek 1989b). However, when the radiation field is not isotropic, for instance when inhomogeneities are present or when macroscopic velocities introduce appreciable Doppler shifts, the integration of R and I over angle and frequency cannot be decoupled and has to be carried out explicitly for all solid angles and the whole frequency domain. Unfortunately, this requires a much larger computational effort, because the redistribution function R in this angle-dependent case has to be tabulated for all possible combinations of four different parameters (two for frequency and two for angle) instead of two and, on a value-by-value basis, is not any cheaper to evaluate than the angle-averaged function.

In the special case of a plane-parallel atmosphere, we can take advantage of the rotational symmetry of the radiation field, leaving just the redistribution function for the integration over azimuth in equation (1). The evaluation of this azimuthally averaged redistribution function, which describes the probabilities for scattering from one elevation angle into another, is discussed in the next section.

2.1. *Plane-Parallel Atmospheres*

In the rotationally symmetric case of a plane-parallel atmosphere, the scattering integral $\mathscr{S}$, which can be defined as

$$\mathscr{S}(\nu, \boldsymbol{n}) = \int_{-\infty}^{\infty} d\nu' \oint \frac{d\Omega'}{4\pi} I(\nu', \boldsymbol{n}') \frac{R^{\mathrm{II}}(\nu, \boldsymbol{n}; \nu', \boldsymbol{n}')}{\phi(\nu, \boldsymbol{n})}, \quad (6)$$

can be rewritten as

$$\mathscr{S}(\nu, \mu) = \frac{1}{2} \int_{-\infty}^{\infty} d\nu' \int_0^{\pi} \frac{\overline{R}(\nu, \mu; \nu', \mu')}{\phi(\nu, \mu)} I(\nu', \mu') d\mu', \quad (7)$$

where μ is the cosine of the angle to the normal direction of the atmosphere, and

$$\overline{R}(\nu, \mu; \nu', \mu') \equiv \frac{1}{2\pi} \int_0^{2\pi} R^{\mathrm{II}}(\nu, \boldsymbol{n}; \nu', \boldsymbol{n}') d\varphi \quad (8)$$

is the azimuthally averaged redistribution function.

Let us consider the azimuthally averaged redistribution function $\overline{R}(\nu, \mu; \nu', \mu')$ describing the probability upon scattering that a photon that is absorbed at frequency ν' and traveling in a conical surface corresponding to μ' is emitted at frequency ν into a conical surface around the vertical with an angle corresponding to μ. To evaluate the azimuthal average of this scattering process, we have to integrate over all the possible relative angles β between rays in the two cones corresponding to μ and μ'. The relation between the relative azimuth φ of two such rays and the relative angle β between them is given by

$$\cos \varphi(\beta) = \frac{\cos \beta - \mu\mu'}{(1 - \mu^2)^{1/2}(1 - \mu'^2)^{1/2}}. \quad (9)$$

The inverse function $\beta(\varphi)$ is symmetric around $\varphi = \pi$ and spans a different range of values depending on μ and μ'. The range of values is largest when both μ values represent rays at large ($\approx \pi/2$) angles from the atmosphere's normal. In this case, the range in values of β varies between back scattering (for $\varphi = 0$) to almost scattering forward (for $\varphi = \pi$). Consequently, the integrand of equation (8) varies substantially with φ. This is illustrated in Figure 1, which shows the angle-dependent redistribution function, normalized with the absorption profile, as a function of relative azimuth angle φ and absorption frequency x' for four different emission frequencies x. For both the incoming and outgoing photon, μ is 0.11. The range in β in this case is between 0 and 0.93π rad for φ varying between 0 and π. By contrast, when $\mu = 0.89$ and $\mu' = 0.11$, β only varies between 0.31π and 0.62π for the same range of φ.

Figure 2 shows the corresponding graphs of the normalized angle-dependent redistribution function, which now only shows very mild variation with relative azimuth φ because the corresponding relative angles correspond mostly to scattering in the neighborhood of 90°.

The numerical integral over azimuth (eq. [8]) can now easily be performed using a Gauss-Legendre quadrature in φ and the inverse of equation (9) to calculate the corresponding values of β. The number of quadrature points required for accurate integration clearly depends on the direction cosines μ and μ'. A denser quadrature is needed when either of the cosines corresponds to a near horizontal ray; a sparser grid will suffice when both the incoming and outgoing photon travel in a near vertical direction. Figure 3 shows the azimuthally averaged redistribution function $\overline{R}(\mu, x; \mu', x')$ as a function of reduced absorption frequency x' for different values of the emission frequency x, when both μ and μ' are small. The two curves represent quadratures of 8 (*dashed line*) and 64 points, respectively. The latter constitutes a sufficiently fine grid that it can be assumed to give the exact result. The largest deviations between the two curves appear near $x' = x$, because the sparser $N_{\mathrm{Gauss}} = 8$ quadrature does not properly sample the narrow peaks in the angle-dependent redistribution function (x' close to x or $-x$ for $x \leq 2$, and β close to 0 or π). When either of the directions μ or μ', or both, correspond to nearly vertical rays, the angle quadrature for sufficient accuracy is sparse, as is evident in Figure 4, which displays the azimuthally averaged redistribution function $\overline{R}(x, \mu; x', \mu')/\phi(x)$ for $\mu = 0.89$ and $\mu' = 0.11$. The sparse $N_{\mathrm{Gauss}} = 8$ grid is sufficiently accurate here for the azimuthal integration. Any remaining error will be taken out almost completely by numerical normalization of the redistribution function.

2.2. *Angle-averaged Redistribution in Moving Atmospheres*

The PRD line emission profile (eq. [1]) is often rewritten using the ratio ρ of the CRD and PRD emission profiles ϕ and ψ, respectively (Uitenbroek 2001):

$$\psi_{ij}(\nu, \boldsymbol{n}) = \rho_{ij}(\nu, \boldsymbol{n}) \phi_{ij}(\nu, \boldsymbol{n}). \quad (10)$$

In the employed numerical scheme, ρ is iterated separately between main iterations to redistribute radiation within each PRD line (Uitenbroek 2001). When the radiation field is sufficiently isotropic, ρ is conveniently evaluated by separating the angle and frequency integration so that the scattering integral is angle-independent and can be written as

$$\mathscr{S}(\nu) = \int_{-\infty}^{\infty} \frac{R(\nu, \nu')}{\phi(\nu)} J(\nu') d\nu'. \quad (11)$$

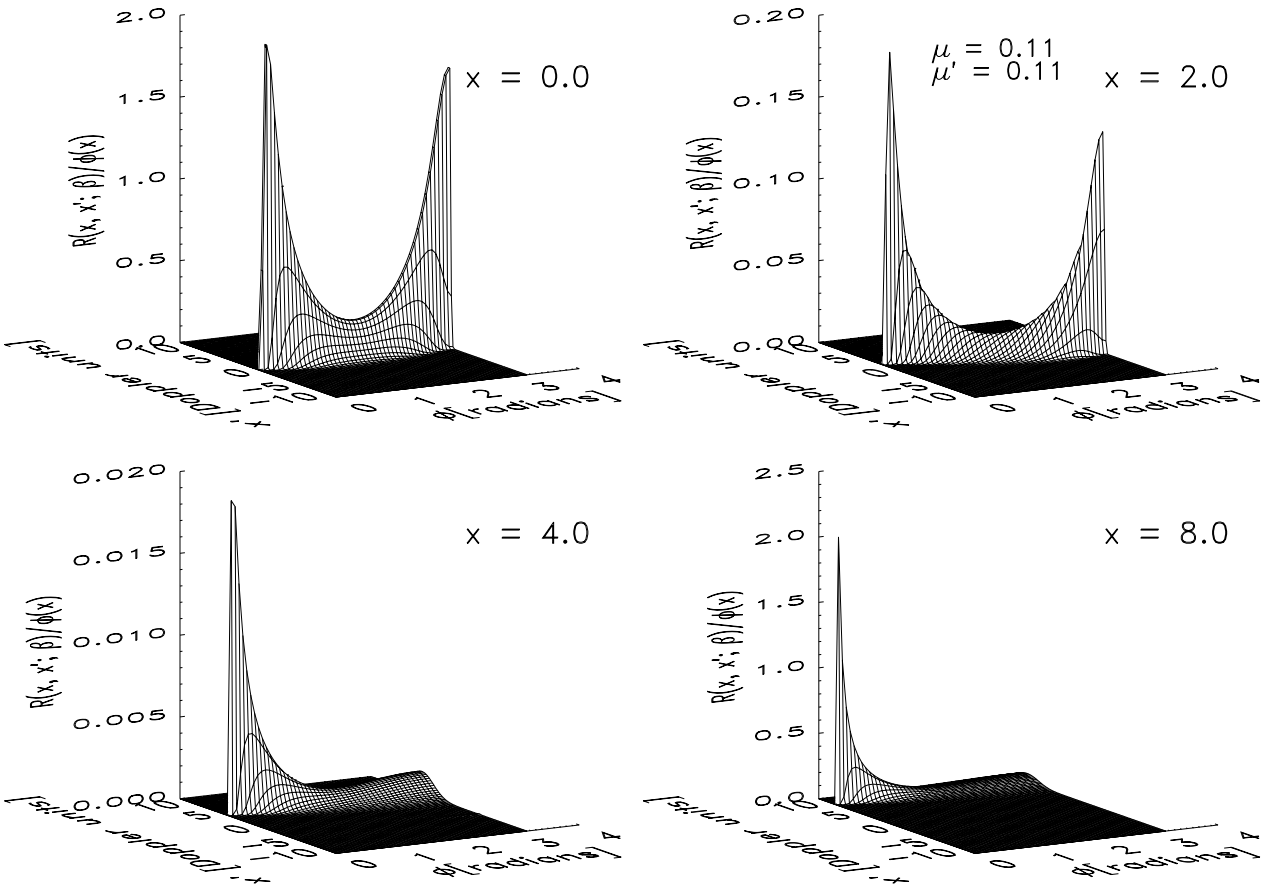


FIG. 1.—Angle-dependent redistribution function (normalized with the CRD emission profile) as a function of azimuthal angle φ and reduced absorption frequency x' (in Doppler units) for four different emission frequencies x ranging from line center $x = 0$ out to 8 Doppler units into the wings. All four surface graphs are for μ and μ' equal to 0.11.

The profile ratio ρ is then given by

$$\rho(v) = 1 + \gamma \frac{n_i B_{ij}}{n_j P_j} [\mathcal{S}(v) - \bar{J}] . \quad (12)$$

To maintain this simple structure in the numerical code when macroscopic velocities $\boldsymbol{v}$ are present and angle-averaged redistribution is deemed sufficiently accurate, we make the following approximation for the Doppler-shifted PRD emission profile:

$$\psi(v - \boldsymbol{v} \cdot \boldsymbol{n}/c) = \rho(v)\phi(v - \boldsymbol{v} \cdot \boldsymbol{n}/c) , \quad (13)$$

with ρ given by equation (12). Thus, we are using the unshifted static redistribution function averaged in the comoving frame, which is a valid approximation if the mean intensity J varies slowly over frequencies comparable to the Doppler shift. This condition is mostly satisfied in the calculations presented here, even though macroscopic velocities are of the order of several times the thermal velocity, amounting to shifts of several Doppler units. With the choice of equation (13), we prevent additional observer's frame averaging of the redistribution function, which may lead to additional broadening and unphysical results (Mihalas et al. 1976). In addition, this choice leads to large savings in computer time because the redistribution function needs to be calculated only once for each (v, v') pair, as opposed to each $(v, \mu; v', \mu')$ pair when using the velocity-dependent angle-averaged redistribution function. The latter would constitute an effort comparable to the evaluation of the angle-dependent redistribution function.

2.3. *Effect of PRD on Emergent K-Line Profiles*

To get an impression of the effect of frequency redistribution on the diagnostic properties of the Ca II K line, we discuss the emerging CRD and angle-averaged and angle-dependent PRD K-line profiles through a hydrostatic model of the quiet Sun and a series of 20 snapshots from a radiation-hydrodynamics simulation. A standard five-level plus continuum representation of ionized calcium was used. This is sufficiently realistic to study the line formation of the H and K lines and the infrared triplet lines accurately. All five lines were treated in detail, as were the radiative bound-free transitions for all five singly ionized calcium levels. Only the two resonance lines were treated with PRD if effects of coherent scattering were considered; the infrared triplet lines were always treated with CRD. The depth-dependent van der Waals broadening was calculated according to the Unsöld approximation with a multiplicative factor of 1.5.

In fitting line profiles in semiempirical models, it is common to invoke free parameters in the form of microturbulence and macroturbulence to match the width and depth of the calculated line with observed profiles. In a priori simulations, such as the radiation hydrodynamics from which the snapshots employed here were taken, the velocities inherent in the dynamics take care of most of the

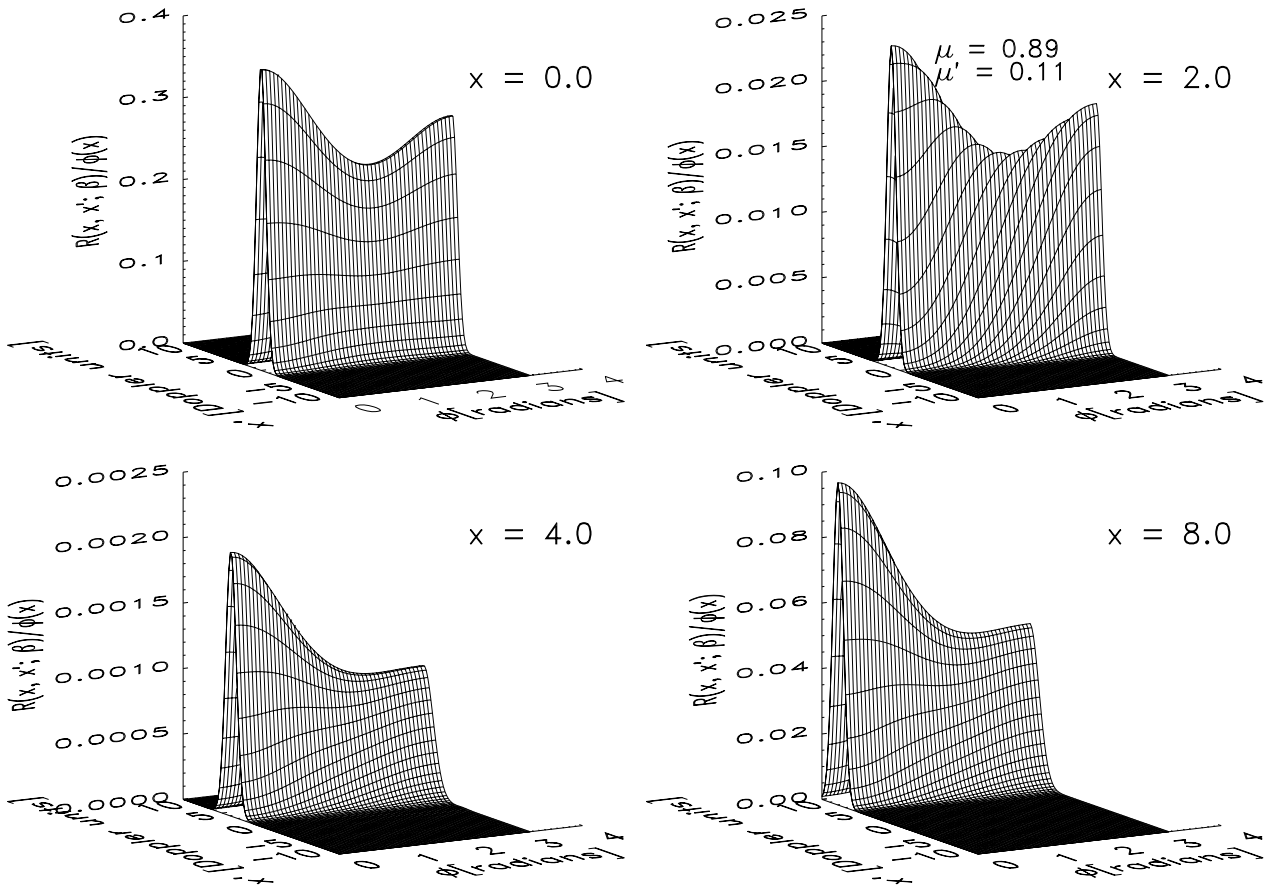


FIG. 2.—Same as Fig. 1, but for cones corresponding to $\mu = 0.89$ and $\mu' = 0.11$

required additional line broadening, although some small amount of broadening may be required because of small-scale motions not resolved in the simulation. Accordingly, we only assume a small amount of microturbulence, a constant 2 km s^{-1} throughout the atmosphere, in the dynamic snapshots. In the hydrostatic model, we take the concurrent microturbulence specified in the model. In both cases, the microturbulent broadening is taken into account, much like thermal broadening, in the calculation of Doppler width and in the damping parameters for the emission and absorption profiles, and the redistribution function.

2.3.1. *Formation in the Hydrostatic Model*

Figure 5 displays the emergent K-line profiles for CRD (*dashed curve*), angle-averaged (*solid curve*), and angle-dependent PRD (*dot-dashed curve*) through the Fontenla et

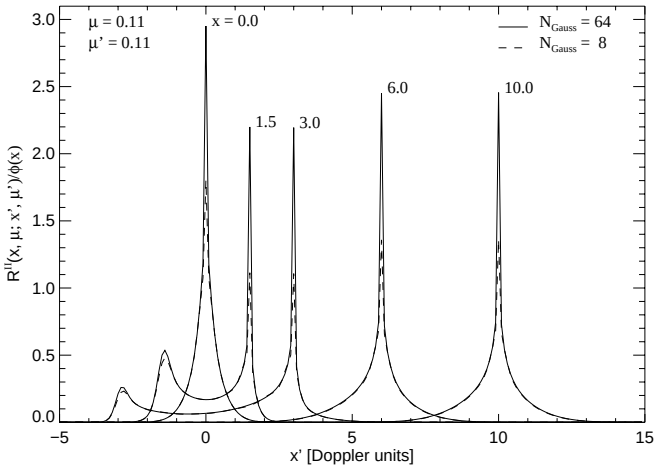


FIG. 3.—Azimuthally averaged redistribution function $\overline{R}(\mu, x; \mu', x')$ [normalized to the CRD emission profile $\varphi(x)$ as a function of reduced absorption frequency x' for five different emission frequencies x ranging from 0 to 10 Doppler units]. The two curves are for different sizes of the angle integration quadrature with eight (*dashed curve*) and 64 points (*solid curve*), respectively. The graphs are for both μ and μ' equal to 0.11.

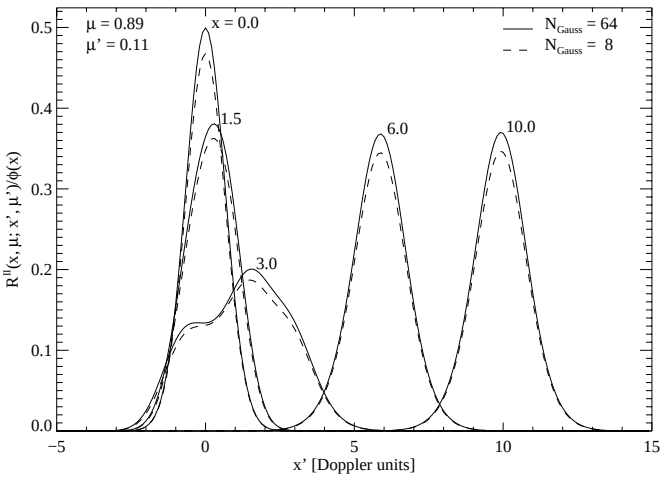


FIG. 4.—Same as Fig. 3, but for $\mu = 0.89$ and $\mu' = 0.11$

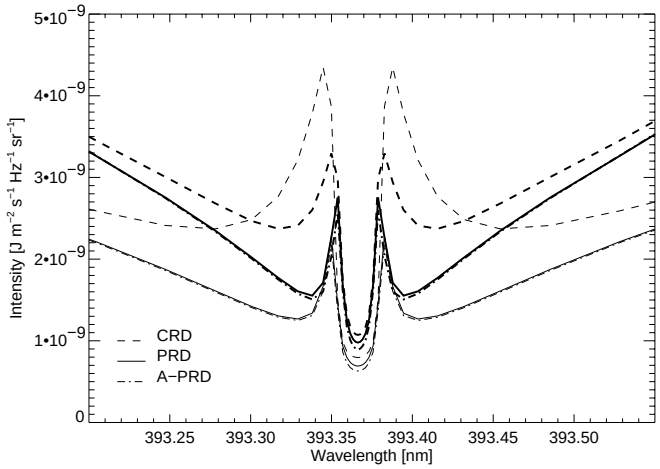


FIG. 5.—Comparison of the inner part of the emergent line profiles of the Ca II K line through the standard FAL-C quiet-Sun model for CRD (*dashed curve*), angle-averaged PRD (*PRD*, *solid curve*), and angle-dependent PRD (*A-PRD*, *dot-dashed curve*). The curves are for two different viewing angles, corresponding to $\mu = 0.95$ (*thick curves*, *almost disk center*) and $\mu' = 0.23$ (*thin curves*, *toward the limb*).

al. (1993) model of the average quiet Sun (their model C, hereafter called FAL-C). The difference between CRD and both PRD profiles is immediately obvious, especially in the behavior of the K_1 relative minima. In CRD, these shift away from line center when viewed toward the limb, while remaining at the same intensity level. With partial redistribution, the minima occur at approximately the same wavelength, but decrease in intensity. The reason for this very different behavior is the wavelength independence of the K-line source function in CRD, which follows the Planck function through the temperature minimum $T_{\rm min}$ in model FAL-C. The K_1 minima in the line profiles at different angles thus all reflect the brightness temperature of $T_{\rm min}$. They shift away from line center at shallower viewing angles because the wavelength at which the temperature minimum is seen (i.e., has optical depth around unity) occurs further and further into the wings. In the PRD case, however, the line source function of the inner wings is decoupled from the Planck function because of coherent scattering. For each wavelength, it levels off outwardly around the location at which the optical depth at that wavelength is unity. There is only one wavelength, symmetrically on both sides of the core, for which the source function decouples in the temperature minimum. The K_1 minima precisely reflect the level of this (almost flat, but slightly decreasing outwardly) source function (e.g., Uitenbroek 1989a), causing the K_1 minima to appear at this wavelength for all viewing angles, with slightly decreasing brightness toward the limb.

In the K_3 core, the CRD profile is slightly brighter than both PRD profiles because the line is able to absorb photons from the wings and reemit them in the core in the outer layers of the atmosphere (corresponding to the upper chromosphere where the absorption profile widens because of increased microturbulence). This is prevented by coherent scattering in PRD, where wing and core photons preferentially keep their character.

Milkey et al. (1975) found very little difference between emergent Ca II resonance line profiles computed with angle-dependent and angle-averaged PRD. This is confirmed in Figure 5: for both viewing angles in this figure, the difference between angle-averaged and angle-dependent redistribution profiles is very small, with the latter being slightly darker in the K_3 core in both instances. In contrast to the constant redistribution function employed by Milkey et al. (1975), the fully depth-dependent redistribution function was used to generate the graph in Figure 5. The difference between the two redistribution formalisms occurs because the angle-dependent treatment properly accounts for the anisotropy in the radiation field in the upper layers of the atmosphere. Since the angle-dependent redistribution function has a larger probability for forward and backward scattering than for intermediate angles (see, for instance, Fig. 1), the radiation anisotropy (due to radiation losses at the surface) increases the probability for photons to be scattered up vertically, where it is easier to escape, instead of toward shallower angles, where it is more difficult to escape due to an increased path length. The greater escape probability slightly lowers the line source function and with it the emergent intensity, enhancing the effect of coherent scattering beyond the angle-averaged case.

2.3.2. *Formation in the Dynamic Snapshots*

When macroscopic velocities are present in the atmosphere, they introduce a coupling between angles and frequencies in the transfer of radiation. This increases the probability that the radiation field is anisotropic, so that we have to consider the case for angle-dependent redistribution more carefully than appears to be necessary for the static plane-parallel case discussed above. To test this assumption, the emergent Ca II K line profiles were calculated for all three different redistribution formalisms through a series of 20 snapshots from a chromospheric-dynamics simulation by Carlsson & Stein (1999), which considers the hydrodynamic evolution of acoustic waves generated at the bottom of the atmosphere. When the acoustic disturbances travel upward through the gravitationally stratified atmosphere, they form shock waves, which heat the atmosphere and produce chromospheric emission. As such, they provide an alternative to classical one-dimensional models, which describe the chromospheric emission as coming from a layer that is always hot and has a monotonically increasing outward temperature rise. The velocities associated with the outwardly traveling shocks in the dynamical simulations are considerable, reaching downward velocities of up to about 15 km s^{-1}, and provide a good test bed for the two PRD formalisms. The whole set of 20 snapshots covers 190 s of real time, comparable to the characteristic periods of waves in the chromosphere, with 10 s between each successive snapshot.

For clarity, Figure 6 only shows a set of four K-line profiles, each 40 s apart in real time, from the whole series of 20 snapshots. As in the previous section, a five-point angle quadrature was used for the evaluation of the radiative rates, approximate operator, and scattering integral. The panels clearly exhibit the effect of a shock wave traveling through the K-line–forming region, giving rise to a prominent K_{2V} brightening in the frames for time $t = 100$ and 120 s. There is considerable difference between CRD (*dashed curves*) and the angle-averaged (*solid curves*) and angle-dependent (*dot-dashed curves*) PRD profiles, especially around the appearance of the K_{2V} emission, when the shock traverses the region where the K_2 emission forms. This region corresponds to the lower chromosphere in the plane-

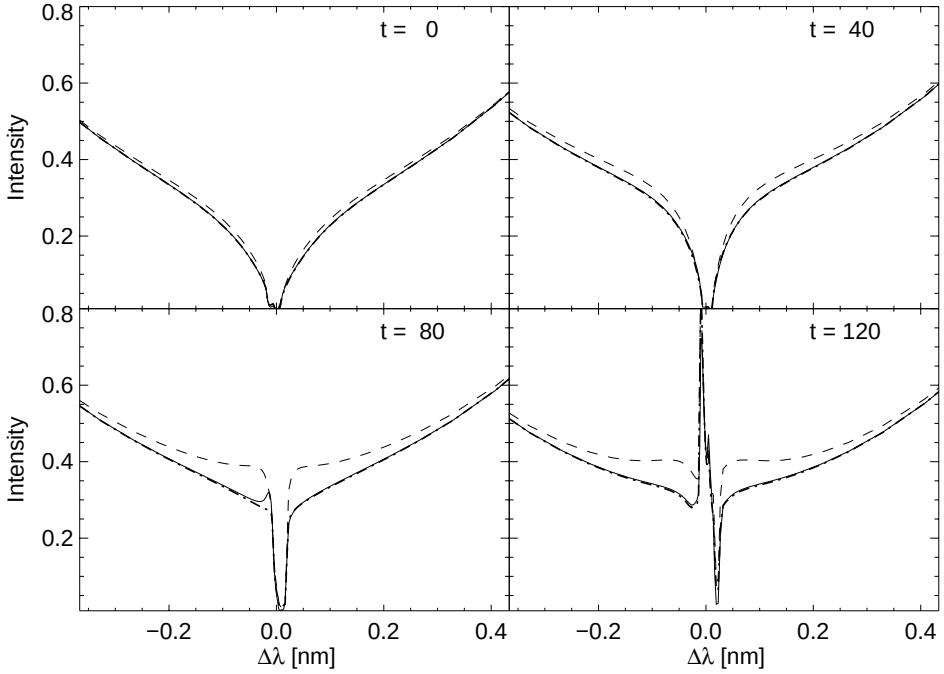


FIG. 6.—Comparison of the inner part of the emergent line profiles of the Ca II K line through a selection from the set of chromospheric dynamics snapshots. Curves are for CRD (*dashed curve*), angle-averaged PRD (*PRD*, *solid curve*), and angle-dependent PRD (*A-PRD*, *dot-dashed curve*). All profiles are for $\mu = 0.95$. Note that $t = 0$ does not refer to the beginning of the simulation starting with an unperturbed atmosphere, but was chosen as a convenient reference time to show the relative times of the consecutive snapshots. The set is characteristic for the dynamics of the atmosphere after the start-up behavior has passed.

parallel hydrostatic models and is the location where the K-line source function decouples from the Planck function and starts to differentiate with wavelength when coherent scattering is taken into account. Again, however, there is very little difference between the two PRD formalisms, with the frame for $t = 80$ s being the only exception. Here the angle-averaged profile already starts to show the K_{2V} emission, while the angle-dependent profile still does not betray the presence of the acoustic disturbance coming from below.

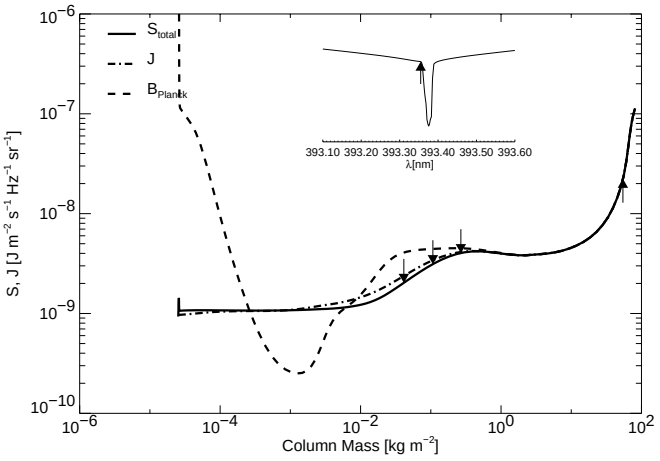


FIG. 7.—Source function of the K line plus continuum at the wavelength indicated by the arrow in the inset. Also plotted are the Planck function (*dashed curve*) and angle-averaged mean intensity J (*dot-dashed curve*) for that wavelength. The downward arrows in the main panel indicate (from left to right) the location of optical depth values 0.3, 1.0, and 3.0 for this direction and wavelength. The upward arrow indicates the location of optical depth unity in the continuum.

The difference between CRD and PRD profiles is straightforward to explain from the source-function structure of the K line in both cases. Figure 7 shows the angle-dependent source function for a near-vertical ray at the wavelength corresponding to the K_2 emission reversals (indicated by the arrow in the inset). The total source function $S_{\rm total}$, which is completely dominated by the line at this wavelength, drops below the Planck function at a column mass of about 0.5 kg m^{-2} because of the photon losses allowed by coherent scattering at this wavelength in the PRD solution. In CRD, the wavelength-independent line source function is coupled to the Planck function out to smaller column masses, causing the inner wings of the CRD solution to be raised above the PRD solution when an acoustic disturbance passes.

Similarly to the plane-parallel case, the angle-dependent redistribution enhances the effect of coherent scattering beyond that of the angle-averaged variant because it facilitates even more the escape of wing photons; when the radiation field becomes anisotropic (i.e., mainly vertical), the preference of the redistribution function for forward scattering enables photons to escape vertically, taking the shortest route, instead of being scattered into shallower angles where it is more difficult for them to escape because of the longer path length through the atmosphere. This effect lowers the angle-dependent PRD source function for the K_2 wavelength enough to prevent the K_{2V} emission from occurring in the $t = 80$ s snapshot.

3. THE RADIATIVE COOLING RATE

Let us now turn to a brief description of the net radiative rate, and then investigate the influence of frequency redistribution on the heating and/or cooling of the solar atmosphere due to the K line. In a line transition between upper

level j and lower level i, the net radiative cooling rate Φ at a given location in the atmosphere due to that line is given by

$$\Phi_{ji} = h\nu(n_j R_{ji} - n_i R_{ij}) . \quad (14)$$

Here R_{ij} and R_{ji} are the upward and downward radiative rates, respectively (see eq. [28] in Uitenbroek 2001):

$$R_{ij} = B_{ij} \oint \frac{d\Omega}{4\pi} \int d\nu \, \phi_{ij}(\nu, \boldsymbol{n}) I(\nu, \boldsymbol{n}) ,$$

$$R_{ji} = A_{ji} + B_{ji} \oint \frac{d\Omega}{4\pi} \int d\nu \, I(\nu, \boldsymbol{n}) \psi_{ij}(\nu, \boldsymbol{n}) . \quad (15)$$

These expressions account properly for the rate of stimulated emission in the case of PRD, in which the emission-profile coefficient ψ is in general not equal to the absorption-profile coefficient ϕ. Using the relations between the Einstein coefficients A and B, we can rewrite the expression in equation (14) in terms of the line source function S_ν^l and opacity χ_ν^l:

$$\Phi_{ji} = \frac{h\nu}{4\pi} \oint d\Omega \int d\nu \times \left[n_j A_{ji} \psi_{ij} - B_{ij} \left(n_i - \frac{g_i \rho_{ij}}{g_j} n_j \right) \phi_{ij} I_\nu \right] = \oint d\Omega \int d\nu \, \chi_\nu^l (S_\nu^l - I_\nu) , \quad (16)$$

where $\rho = \psi/\phi$ is the ratio of emission- and absorption-profile coefficients. When more photons are emitted than absorbed in a line transition in a certain volume of plasma, Φ is positive, and that volume is radiatively cooled by the line. When Φ is negative, the volume is said to be heated by the radiation in the line.

3.1. *Cooling in Hydrostatic Solar Models*

To get some insight into the cooling action of the H and K lines and how it is affected by the choice of redistribution formalism, let us first turn to a comparison between radiative cooling under CRD, angle-averaged, and angle-dependent PRD in the standard plane-parallel hydrostatic solar model FAL-C. A five-point Gauss-Legendre quadrature in μ was used for the viewing angles. Any difference we find in the respective cooling rates for the given atmospheric structure in the model has implications for the amount of mechanical heating and/or cooling we presume is necessary to support the atmosphere's temperature structure. Figure 8 shows the radiative cooling by the Ca II K line as a function of column mass for the three different redistribution formalisms. The figure displays similar information to what is presented in Figure 49 of Vernazza et al. (1981) for a number of different lines, including the K line, which was calculated with the simple approximation of the $R^{\rm II}$ redistribution function given by Kneer (1975). Using the full depth-dependent redistribution function, we find, as in the case of the emerging line profiles, negligible difference between angle-averaged and angle-dependent PRD. This is true throughout the atmosphere. The difference between the CRD and PRD cooling rates, however, is considerable; the K line is radiatively heating the atmosphere between column mass $m = 0.5$ and 6 kg m^{-2} in the complete redistribution case, while the line provides cooling in that region when coherent scattering is taken into account. For optical

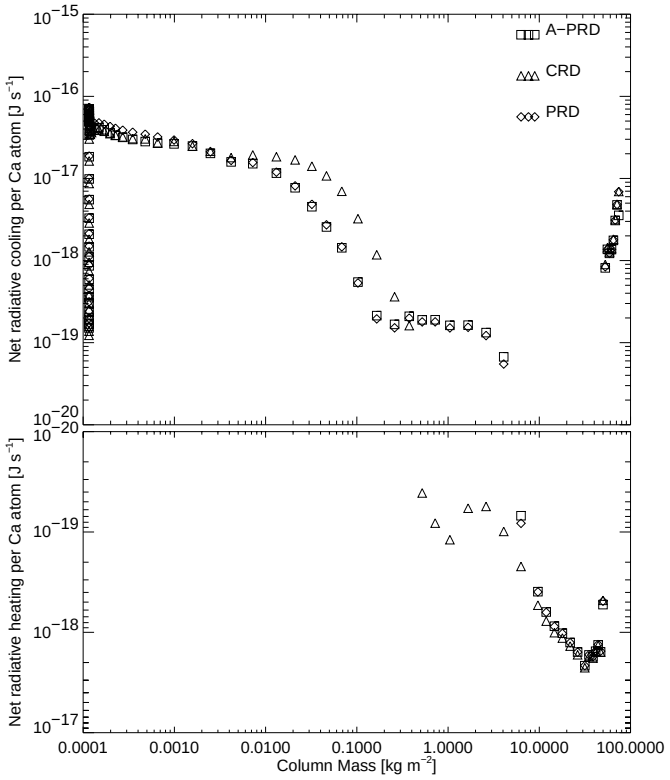


FIG. 8.—Net radiative cooling (*top panel*) and heating (*bottom panel*) per calcium atom due to the Ca II K line in the average quiet-Sun model FAL-C for the three different redistribution cases: angle-dependent PRD (*squares*), CRD (*triangles*), and angle-averaged PRD (*diamonds*). The net radiative rates are normalized with the calcium number density.

depths between $m = 0.01$ and 0.5 kg m^{-2}, the lines provide more cooling in CRD than in PRD by a factor of 2–5.

In the temperature minimum region, around $m = 1.0$ kg m^{-2} in model FAL-C, the K line is heating the atmosphere through its wings because $J > S$ at those wavelengths and that depth. Closer to the core, both the PRD and CRD source function run above J in the $T_{\rm min}$ region, so that the inner wings (around K_1) always provide cooling. In PRD, the wing heating is small and not enough to offset the core cooling, because coherent scattering forces S to be close to J. In CRD, however, the difference between S and J is much larger in the wings, because the CRD line source function follows the Planck function through the temperature minimum, while the mean intensity J in the wings has already been decoupled deeper in the atmosphere, so that it runs at much higher values than the source function. In this case, the wing heating more than compensates for the cooling in the core, causing the sign reversal of the net radiative cooling.

In the lower chromosphere, the CRD source function starts to decouple from the Planck function, but it is still closer to the outwardly increasing Planck function than the PRD source function at the wavelength of the K_2 relative maxima, which provide the radiative cooling for column masses between 0.5 and 0.01 kg m^{-2}. The mean intensity J is approximately the same in both cases, so that the larger difference between J and S in CRD results in a larger net radiative cooling in this region.

The differences obtained here between the CRD and PRD cooling curves for the K line are very similar in character to the differences described by Huenerth & Ulmsch-

neider (1995) for the Mg II k line in the older Vernazza et al. (1981) quiet-Sun model. The magnesium line does not show a net heating in CRD in the lower chromosphere, probably because the wing heating is smaller; because of the larger opacity of the magnesium line, $J_{\rm wing}$ is coupled closer to the Planck function at these heights.

3.2. *Cooling in a Chromospheric Dynamics Simulation*

In radiation-hydrodynamics simulations, such as the one by Carlsson & Stein (1999), the temperature, density, and ionization structure are determined by the balance between radiative and mechanical sinks and sources. One of the major energy loss mechanisms in the upper atmosphere is radiative cooling in strong lines, such as the hydrogen Hα line and the Ca II H and K and infrared triplet lines (Vernazza et al. 1981, Figs. 48 and 49). Considering the large differences between the emergent CRD and PRD profiles of the K line discussed in §§ 2.3.1 and 2.3.2, we investigate here how frequency redistribution affects the radiative cooling and/or heating by this line. Through each of the 20 snapshots from the dynamic simulation, radiative transfer was solved for the Ca II model for the three different redistribution formalisms. Subsequently, the net radiative rates for the K line were evaluated according to equations (14) and (15). Since CRD was used originally in the simulation to calculate the radiative K-line losses, the determined cooling rate assuming PRD in this way is unrealistic, at least when it differs considerably from the CRD rate. The temperature structure of the atmosphere would most likely have been different had PRD cooling been applied; in general, we would expect that the atmosphere would be hotter if cooling in PRD was less than in CRD, and vice versa. A quantitative comparison between CRD and PRD can thus only be made by comparing radiative losses from different simulations that use either of the redistribution descriptions to calculate the actual contributions to the energy balance. Here we can only indicate in what way the losses are expected to be different.

We find indeed that radiative losses are probably significantly different between PRD and CRD. Figure 9 shows the cooling curves for the snapshots at $t = 0$ (*left panel*) and $t = 80$ s. Remarkably, although the emerging profiles are very similar for the first case (see the top left panel in Fig. 6), when the acoustic disturbance is still deep in the atmosphere, the net radiative rates are substantially different, especially higher up in the atmosphere, where the K line provides considerably more heating in CRD than in PRD. In this region, the CRD source function in the wings is coupled to the low-temperature Planck function and runs well below the mean intensity J, implying strong wing heating. By contrast, in the PRD case, the wing source function closely follows J because of the coherency of scattering, reducing the heating by the line. In both CRD and PRD, the cooling at core wavelengths is not strong enough to overcome wing heating because of the extended low-temperature region in this phase of the simulation. Differences between angle-averaged and angle-dependent PRD are small throughout the whole atmosphere at this instant of time.

About half a typical chromospheric oscillation period later, at $t = 80$ s, the acoustic wave has progressed to the K_2-forming region, and the cooling curves look very different (right panel of Fig. 9). Behind the disturbance, between column mass $m = 0.03$ and 2.0 kg m^{-2}, the CRD cooling is up to a factor of 3 larger than with PRD. In front of the disturbance, the picture is similar to earlier times, such as

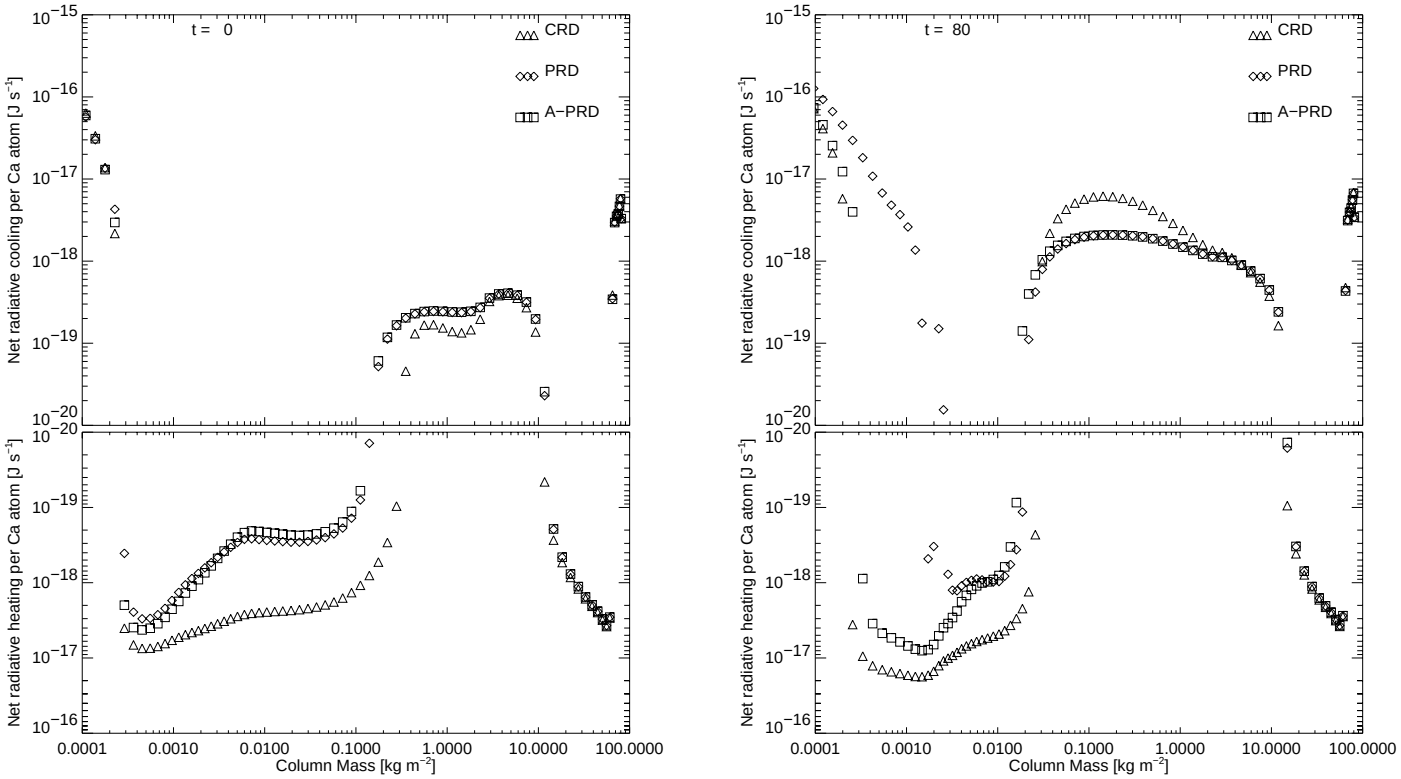


FIG. 9.—Net radiative cooling curves in two dynamic snapshots ($t = 0$ and 80 s) for CRD (*triangles*) and angle-averaged (*diamonds*) and angle-dependent PRD (*squares*).

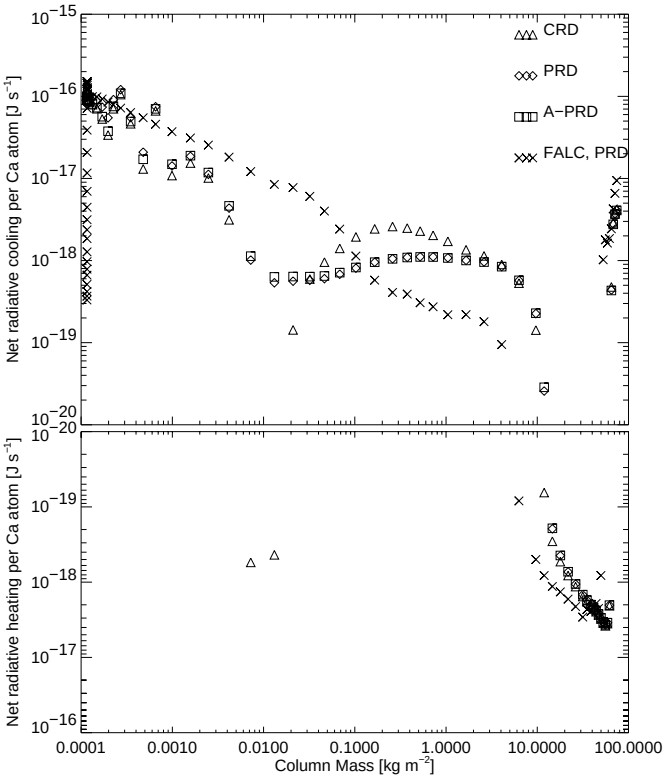


FIG. 10.—Time-averaged cooling curves of the 20 dynamic snapshots, spanning 190 s in real time, for CRD (*triangles*) and angle-averaged (*diamonds*) and angle-dependent PRD (*squares*). Also shown is the FAL-C cooling curve for angle-averaged PRD (*crosses*).

$t = 0$, with CRD providing larger heating. In the deeper layer, the PRD wing source function falls below the raised Planck function (corresponding to the higher temperature behind the disturbance), but not as much as the mean intensity J. Thus, $S > J$, which means radiative cooling. In CRD, the wing source function still follows the outwardly increasing Planck function closely, so that the difference between it and J are larger than in PRD, giving rise to higher net cooling rates. At this later time, there is also a large difference between angle-dependent and angle-averaged redistribution for layers around $m = 0.001$. This is due to the large downward velocity (-9 km s^{-1} at about $m = 0.001$, with a steep outward increase to zero at the top of the atmosphere) associated with the acoustic disturbance. In both redistribution formalisms, the core is cooling the atmosphere, and in angle-averaged redistribution, both the red and blue wing are heating the atmosphere by a much larger amount, just as in the CRD case in the temperature minimum of model C. At $t = 80$ s in the dynamical simulation, however, the blue inner wing of the K line cools the atmosphere around $m = 0.001$ enough to compensate for the heating in the red wing, so that with the core cooling, the net radiative rate (eq. [14]) is positive in angle-dependent PRD. The reason for this is that the source function of the blue wing is mostly determined by radiation coming from below, which is blueshifted with respect to the local comoving frame. The wing thus "sees" the brighter wing radiation, rather than the darker core radiation, and its source function is raised above the mean intensity, implying cooling.

Considering the fact that radiative cooling and heating rates may be both larger and smaller in PRD than in CRD, the question arises how much the time-averaged cooling curves differ between the two formalisms.

The mean cooling curves of the 20 snapshots are shown in Figure 10 for CRD (*triangles*), angle-averaged redistribution (*diamonds*), and angle-dependent redistribution (*squares*), together with the angle-averaged PRD cooling curve for model FAL-C. This figure shows indeed that most of the differences between the different redistribution formalisms average out over time, apart from the excess cooling in the CRD case between $m = 0.1$ and 1.0. The figure also shows that, on average, the K line provides more cooling in the classical temperature-minimum region in the dynamic simulation than it does in the hydrostatic model, but the line provides less cooling in the lower chromosphere (above $m = 0.1$).

4. CONCLUSIONS

Expressions for the evaluation of the angle-dependent and azimuthally averaged redistribution function (eq. [8]), the corresponding scattering integral (eq. [6]), and the approximation for angle-averaged redistribution in moving atmospheres (eq. [13]) are straightforward to implement in the multilevel accelerated lambda iteration code for PRD described by Uitenbroek (2001), without loss of efficiency in the convergence. With this implementation, the importance of the coupling between angles and frequencies in frequency redistribution can now be efficiently investigated in static as well as moving atmospheres. Here we have applied the method to explore the differences in radiative losses due to the Ca II K line under CRD and PRD with and without angle dependence, both in a hydrostatic model of the quiet Sun (Fontenla et al. 1993) and through a series of snapshots from a radiation-hydrodynamic simulation of the nonmagnetic atmosphere (Carlsson & Stein 1999).

It is clear from our calculations that hydrostatic as well as radiation hydrodynamic models of the solar atmosphere suffer significantly in reliability when coherent scattering effects are ignored for the Ca II resonance lines. This holds true for the diagnostic value of emergent line profiles (Figs. 6 and 5) as well as for evaluation of the energy balance (Figs. 8 and 9). In general, employing the approximation of complete redistribution will result in an overestimate of net radiative cooling *and* heating due to the K line. Under PRD, a certain fraction of photons is allowed to scatter coherently, and thus does not contribute to the net radiative rate. In the wing of the line, coherent scattering results in a source function that is generally closer to the mean intensity J than in CRD, reducing the difference between S and J, and thus the absolute value of the net radiative rate (eq. [16]). A similar result was obtained by Huenerth & Ulmschneider (1995) for the Mg II k line.

In the hydrostatic model (Fig. 8) as well as in the time average of the dynamical snapshots (Fig. 10), the difference between the angle-averaged and angle-dependent radiative rates is small. At specific times in the dynamic simulations, however, there may be considerable disagreement between the two formalisms. Differences between CRD and PRD, by contrast, stand out clearly, especially in the temperature-minimum region (column mass m between 0.1 and 1.0), even in the temporal average. Here radiative cooling in the K line is larger in CRD by a factor of 3 (with the caveat that the simulation used CRD to determine the structure that is used here to calculate the PRD radiative rates). On average, cooling rates in the K line in the dynamic chromospheric

model are larger than in the hydrostatic model in the temperature minimum, and less in the chromosphere (Fig. 10).

It appears that the strategy for angle-averaged PRD in a moving atmosphere that is formulated in § 2.2 provides an accurate presentation of PRD in the K line. The calculated emergent profiles differ very little from the full angle-dependent solution at all times in the considered dynamical simulation. The net radiative rates at times are different, but only at the top of the atmosphere, where the radiation field becomes anisotropic and where cooling by the Ca II K line plays a relatively minor role compared to, for instance, the Mg II *k* line (Vernazza et al. 1981, Fig. 49). In the time average through the dynamic snapshots, the curves for the net radiative rates for the angle-dependent and angle-averaged formulation are almost indiscernible (Fig. 10). This holds good promise for dynamical calculations, for which the calculations presented by Huenerth & Ulmschneider (1995) and the results of this paper seem to indicate that some form of PRD is necessary to produce accurate radiative gains and losses in strong resonance lines such as H and K, and the *h* and *k* lines of magnesium. With the formulation given in equation (13), the effects of coherent scattering can easily be implemented, even in a code that uses explicit linearization. In the linearization step, the profile ratio ρ can be taken from the previous iteration and does not have to be linearized. In between main iteration steps, ρ can be updated by successive formal solutions, while keeping the population numbers fixed. This "pseudo" lambda iteration works well and should converge rapidly (Uitenbroek 2001). Even in a moving atmosphere, solving the transfer problem in this way does not require much more work than an angle-averaged PRD solution in a static atmosphere.

It is a pleasure to thank Mats Carlsson and Bob Stein for providing the snapshots from their radiation-hydrodynamics simulation.

REFERENCES

Bruls, J. H. M. J., & Solanki, S. K. 1997, A&A, 325, 1179
Carlsson, M., & Stein, R. F. 1992, ApJ, 397, L59
———. 1995, ApJ, 440, L29
———. 1999, in AIP Conf. Proc. 471, Solar Wind 9, ed. S. R. Habbal (New York: AIP), 23
Fontenla, J. M., Avrett, E. H., & Loeser, R. 1991, ApJ, 377, 712
———. 1993, ApJ, 406, 319
Gouttebroze, P. 1986, A&A, 160, 195
Hubený, I. 1982, J. Quant. Spectrosc. Radiat. Transfer, 27, 593
Hubený, I., & Lites, B. W. 1995, ApJ, 455, 376
Huenerth, G., & Ulmschneider, P. 1995, A&A, 293, 166
Hummer, D. G. 1962, MNRAS, 125, 21
Kneer, F. 1975, ApJ, 200, 367
Maltby, P., Avrett, E. H., Carlsson, M., Kjeldseth-Moe, O., Kurucz, R. L., & Loeser, R. 1986, ApJ, 306, 284
Mihalas, D. 1978, Stellar Atmospheres (2d ed.; San Francisco: Freeman)
Mihalas, D., Shine, R. A., Kunasz, P. B., & Hummer, D. G. 1976, ApJ, 205, 492
Milkey, R. W., Shine, R. A., & Mihalas, D. 1975, ApJ, 202, 250
Rammacher, W., & Ulmschneider, P. 1992, A&A, 253, 586
Shine, R. A., Milkey, R. W., & Mihalas, D. 1975, ApJ, 199, 724
Uitenbroek, H. 1989a, A&A, 213, 360
———. 1989b, A&A, 216, 310
———. 2001, ApJ, 557, 389
Vernazza, J. E., Avrett, E. H., & Loeser, R. 1981, ApJS, 45, 635